ACS OMEGA

Article

Cite This: ACS Omega 2018, 3, 10471−10480

http://pubs.acs.org/journal/acsodf

Ultrasensitive Colorimetric and Ratiometric Detection of Cu^{2+}: Acid−Base Properties, Complexation, and Binding Studies

Daniel J. Fanna,[†,#] Luís M. P. Lima,[‡] Alexander R. Craze,[†] Adrian Trinchi,[§] Richard Wuhrer,[∥] Leonard F. Lindoy,[⊥] Gang Wei,[#] Jason K. Reynolds,*[,†] and Feng Li*[,†]

[†]School of Science and Health, Western Sydney University, Locked Bag 1797, Penrith, New South Wales 2751, Australia

[‡]Instituto de Tecnologia Química e Biológica António Xavier, Universidade Nova de Lisboa, Av. da República, 2780-157 Oeiras, Portugal

[§]CSIRO Manufacturing, Private Bag 33, Clayton, Victoria 3169, Australia

[∥]Advanced Materials Characterisation Facility, Western Sydney University, Locked Bag 1797, Penrith, New South Wales 2751, Australia

[⊥]School of Chemistry, University of Sydney, Sydney, New South Wales 2006, Australia

[#]CSIRO Manufacturing, P.O. Box 218, Lindfield, New South Wales 2070, Australia

Supporting Information

ABSTRACT: Herein, we report the synthesis and characterization of a chemosensor, 5-(diethylamino)-2-(2,3-dihydro-1*H*-perimidin-2-yl)phenol (**HL**), synthesized from a condensation between 4-(diethylamino)salicylaldehyde and 1,8-diaminonaphthalene. Upon investigation of the sensing properties of **HL**, it was found that this sensor may be employed for simple yet efficient detection of Cu^{2+} in aqueous methanol solutions. The selective and ratiometric response to Cu^{2+} yielded an outstandingly low limit of detection of 3.7 nM by spectrophotometry and is also useful as a naked-eye sensor from 2.5 μM. The system was studied by spectrophotometric pH titrations to determine Cu^{2+} binding constants and complex speciation. Binding of Cu^{2+} to **HL** occurs in 1:1 stoichiometry, in good agreement with high-resolution electrospray ionization mass spectrometry (ESI-HRMS) results, Cu^{2+} titrations, and Job's plot experiments, while the coordination geometry was tentatively assigned as square pyramidal by spectroscopic studies.

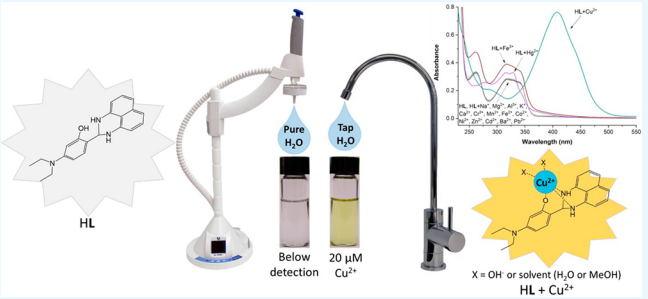

INTRODUCTION

The design and synthesis of new chemosensors for the detection of trace metals, anions, and small molecules continue to be strongly pursued due to their potential for use in medical, biological, industrial, and environmental applications.[1−16] Currently, the detection of biologically active metals such as $Fe^{2+/3+}$,[17,18] Cd^{2+},[19,20] Hg^{2+},[21,22] and Cu^{2+}[23−26] is receiving considerable attention due to their possible adverse effects on human health.[27] Of these metals, copper is the third most abundant transition metal found in humans and plays an essential role in several cuproenzymes.[28] However, free copper is also able to oxidize cellular components through its redox activity, damaging nucleic acids, proteins, and lipids.[29] Hence, an imbalance of copper may be detrimental to human health, causing pathogenesis such as Parkinson's disease, Alzheimer's disease, Wilson's disease, Menkes disease, and Amyotrophic Lateral Sclerosis (ALS).[30−32] In particular, copper is a common pollutant due to its widespread usage in industry, agriculture and drinking water systems. The World Health Organization (WHO) has advised that 2 ppm (31.5 μM) is the recommended upper level for copper in drinking water.[33] Although a considerable number of chemosensor systems have been developed for copper(II) ions (Table 1), the design and successful construction of ultrasensitive and highly selective systems, particularly those with naked-eye detection ability, still represents a significant challenge.

Herein, we report a potential chemosensor, **HL** (Scheme 1), capable of extremely fast colorimetric and ratiometric detection of Cu^{2+} with an impressively low detection limit of 3.7 nM. Detection of copper at low micromolar levels is also possible in the absence of a spectrophotometer, as the visible response of **HL** to Cu^{2+} is significant. Spectrophotometric acid−base studies were carried out in addition to several UV−vis-based metal detection assays, ESI-HRMS, and electron paramagnetic resonance (EPR) studies in order to probe the nature of the binding of **HL** to Cu^{2+} in terms of its sensing ability for this metal ion.

RESULTS AND DISCUSSION

Synthesis and Structure of HL. **HL** was synthesized from the condensation of 4-(diethylamino)salicylaldehyde and

Received: June 28, 2018
Accepted: August 20, 2018
Published: September 4, 2018

DOI: 10.1021/acsomega.8b01483
ACS Omega 2018, 3, 10471−10480

Table 1. Literature Examples of Cu^{2+} Colorimetric and Fluorescent Sensors Including from the Current Work, Ordered by Increasing Sensitivity as Given by the Reported Limit of Detection (LoD)

detection method	media	LoD (nM)	ref
UV−vis	DMF/bis-tris buffer (7:3, v/v, 10 mM bis-tris, pH 7.0)	3890	34
UV−vis	Bis-tris buffer/H_2O (999:1, v/v)	2700	35
UV−vis	DMF/bis-tris buffer (1:1, v/v, pH 7.0)	880	36
UV−vis	Tris-HCl buffer/EtOH (1:1, v/v, 10 mM tris-HCl, pH 7.0)	500	37
UV−vis	DMSO/Bis-tris buffer (1:1, v/v)	360	38
UV−vis	DMSO/Bis-tris buffer (3:2, v/v, 10 mM bis-tris, pH 7.0)	200	39
fluorescence	MeOH/H_2O (2:8, v/v)	314 and 184	40
UV−vis	MeOH/HEPES buffer (1:1, v/v, pH 7.4)	140	41
fluorescence	HEPES buffer/CH_3CN (3:2, v/v, 100 mM HEPES, pH 7.2)	110	42
UV−vis	DMSO/HEPES buffer (9:1, v/v, pH 7.0)	100	43
UV−vis	CH_3CN	61.9	44
fluorescence	EtOH/HEPES buffer (8:2, v/v, 20 mM HEPES, pH 7.2)	40	45
fluorescence	CH_3CN/tris-HCl (1:1, v/v, 10 mM tris-HCl, pH 7)	40	46
UV−vis	CH_3CN/H_2O (varying ratio)	40	47
fluorescence	DMF/HEPES buffer (3:7, v/v, 20 mM HEPES, pH 7.4)	15	48
fluorescence	Tris buffer (25 mM, pH 7.4)	11.2	49
UV−vis	CH_3CN	7.8 and 5.7	50
UV−vis	CH_3CN/Tris buffer (1:1, v/v, 10 mM Tris, pH = 7.0)	5.2, 4.9, and 4.5	51
fluorescence	CH_3CN/MeOH/H_2O (1:9:10, v/v/v)	4 and 3	52
UV−vis	**MeOH/HEPES buffer (1:1, v/v, 20 mM HEPES, pH 7.00)**	**3.7**	**This work**
fluorescence	CH_3CN	2.3	53
UV−vis/ fluorescence	CH_3CN	1.9, 1.8, and 1.7	54
fluorescence	H_2O/CH_3CN (2:1, v/v)	1.45	55
fluorescence	HEPES buffer (20 mM, pH 7.0)	1.1	56
fluorescence	Britton−Robinson buffer/CH_3CN (9:1, v/v, pH = 7.02)	0.739	57

1,8-diaminonaphthalene in isopropanol in the presence of a catalytic amount of *p*-toluenesulfonic acid, as shown in Scheme 1. It was characterized via ^1H and ^{13}C NMR, ESI-HRMS, FT-IR, and STA (simultaneous thermal analysis) techniques (Figures S1−S5). Single crystal X-ray diffraction (SC-XRD) studies demonstrate that HL crystallizes in the orthorhombic *Pbcn* space group, with cell dimensions of a = 25.524(5) Å, b = 13.835(3) Å, c = 9.914(2) Å, and α, β, γ = 90°. A typical bifurcated hydrogen bond is also observed between the hydroxide proton (O1H) and the dihydroperimidine nitrogens (N1 and N2). These hydrogen bonds appear to result in the dihydroperimidine nitrogens being positioned slightly above the plane of the naphthalene ring and twist the plane of the salicyl moiety so that the naphthalene and salicyl ring systems are almost perpendicular (Figure 1). Both edge-to-face and face-to-face π-contacts are present in the lattice between the naphthalene moieties (Figure S6). Crystallographic data is summarized in Table S1, and detailed crystallographic information can also be found in the Supporting Information.

Screening of Metal Cations. The interaction with common metal cations was investigated using 20 μM solutions of HL in a MeOH/H_2O (1:1, v/v; HEPES, 20 mM; pH = 7.00) mixture by addition of two equivalents (40 μM) of the cations. In the presence of Cu^{2+}, the absorbance spectrum develops immediately a strong absorption at 408 nm ($\varepsilon = 3.815 \times 10^4\ M^{-1}\ cm^{-1}$) associated with generation of a yellow color (Figure 2). Small peak changes were also observed for Hg^{2+} and Fe^{3+}, but importantly no other cations gave rise to an intense band centered at 408 nm as observed for Cu^{2+}. The sensing mechanism likely involves a dual ligand-to-metal charge transfer (LMCT) transition (an intense band at 408 nm) characteristic of a Cu^{2+} center coordinated to a phenoxyl[58−60] and naphthalene amine based[61,62] ligand such as HL, which also incorporates an electron donor diethylamino group.

Acid−Base Equilibrium Studies. To characterize the acid−base properties of HL and investigate its interaction with Cu^{2+}, pH titrations monitored by UV−vis spectrophotometry were performed for HL alone and in the presence of Cu^{2+}. The main spectral features of HL varying with a change of pH are the composite band at 310−350 nm assigned to a intraligand $\pi-\pi^*$ charge transfer (CT) transition from phenol and phenolate,[58] the shifting band at 260−280 nm assigned to a intraligand $\pi-\pi^*$ charge transfer (CT) from naphthalene amine,[61,62] and the increasing absorption band at 230 nm (Figure S7a). The spectral variations were fitted to a speciation model containing three protonation equilibria (Figure S7b), and the protonation equilibrium constants obtained are presented in Table 2. The highest protonation detected occurs around pH = 11 and is associated with moderate spectral change, being assigned to protonation of the phenoxyl group as found in similar

Scheme 1. Synthesis of HL

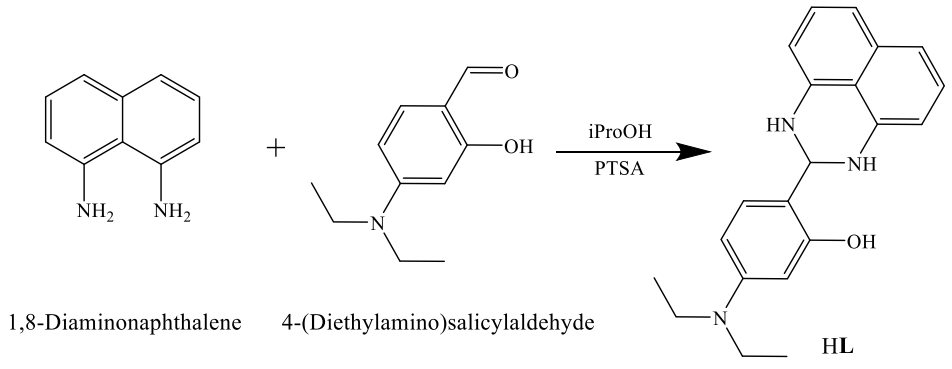

1,8-Diaminonaphthalene 4-(Diethylamino)salicylaldehyde

DOI: 10.1021/acsomega.8b01483
ACS Omega 2018, 3, 10471−10480

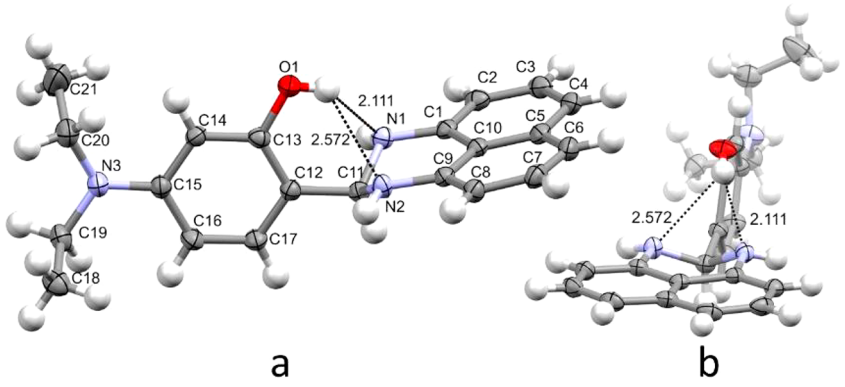

Figure 1. Thermal ellipsoid structure of HL drawn at 50% probability: (a) side view; (b) top view. Bifurcated hydrogen H-bonding represented by dotted lines.

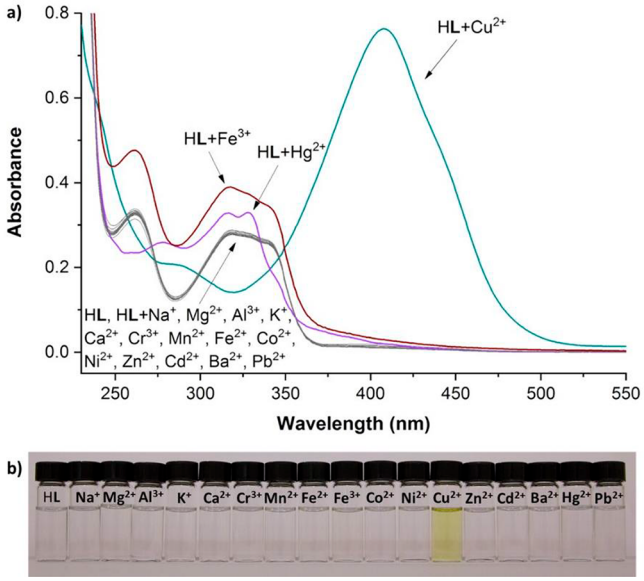

Figure 2. (a) UV−vis absorbance spectra of HL (20 μM) in a MeOH/H_2O (1:1, v/v; HEPES, 20 mM; pH = 7.00) mixture in the presence of two equivalents (40 μM) of common metal ions. (b) Color changes observed by the naked-eye, colorimetric detection for Cu^{2+} (yellow), while solutions of HL and HL plus other cations are all colorless.

functions.[63] Around pH = 5.5, there is an intense spectral change likely associated with protonation of the tertiary amine attached to the phenoxyl group. Below pH = 3.5, there is a very small spectral change possibly arising from protonation of one of the secondary amines of the dihydroperimidine group.

In the presence of an equimolar amount of Cu^{2+}, the UV−vis spectrum of HL changes significantly on moving from acidic to basic pH with a new band developing centered at ca. 408 nm (Figure S8). The spectral variations were in this case successfully fitted to a speciation model containing three complex species corresponding to different protonation states (Figure 3), and the complexation equilibrium constants obtained are presented in Table 2. It should be stressed that all complex species found are of 1:1 metal-to-ligand ratio. At lower pH, the complex exists mainly as the species $[CuHL]^{2+}$, while around and above neutral pH, there are two hydroxo species formed likely from deprotonation of water molecules coordinated to the metal center. It is worth noticing that the $[CuL]^{+}$ species was not obtained in the data fitting, suggesting that it may only exist in very low abundance in equilibrium, if at all. Thus, what is observed

Table 2. Overall (log β) and Stepwise (log K) Thermodynamic Equilibrium Constants[a] for the Protonation of HL and Its Complexation with Cu^{2+} at 25.0 ± 0.1° C in MeOH/H_2O (1:1, v/v) Medium at 0.10 ± 0.01 M in KCl

equilibrium	log β	equilibrium	log K
$L^- + H^+ \rightleftarrows HL$	10.93(1)	$L^- + H^+ \rightleftarrows HL$	10.93(1)
$L^- + 2H^+ \rightleftarrows (H_2L)^+$	16.50(1)	$HL + H^+ \rightleftarrows (H_2L)^+$	5.57(1)
$L^- + 3H^+ \rightleftarrows (H_3L)^{2+}$	19.85(4)	$(H_2L)^+ + H^+ \rightleftarrows (H_3L)^{2+}$	3.35(4)
$Cu^{2+} + L^- + H^+ \rightleftarrows [CuHL]^{2+}$	19.11(1)	$[CuL]^+ + H^+ \rightleftarrows [CuHL]^{2+}$	–
$Cu^{2+} + L^- \rightleftarrows [CuL]^+$	*b*	$Cu^{2+} + L^- \rightleftarrows [CuL]^+$	–
$Cu^{2+} + L^- \rightleftarrows [CuLH_{-1}] + H^+$	10.52(1)	$CuL(OH) + H^+ \rightleftarrows [CuL]^+$	–
$Cu^{2+} + L^- \rightleftarrows [CuLH_{-2}]^- + 2\,H^+$	1.01(3)	$[CuL(OH)_2]^- + H^+ \rightleftarrows [CuL(OH)]$	9.51(3)

[a]Values in parentheses are standard deviations in the last significant figures. [b]Not determined.

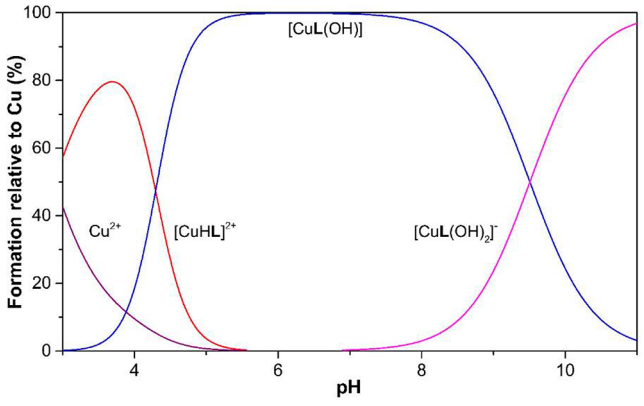

Figure 3. Species distribution diagram for HL in the presence of 1 equiv of $CuCl_2$ versus pH (at 25 μM in MeOH/H_2O 1:1).

corresponds to a double deprotonation step of the complex from $[CuHL]^{2+}$ to $[CuL(OH)]$ around pH = 4−5. The complexation constants obtained for this system evidence a high thermodynamic stability of the complex formed between HL and Cu^{2+}, also resulting in the almost complete absence of free Cu^{2+} above pH = 5 (Figure 3) under the conditions employed.

Cu^{2+} Detection Performance. The stoichiometry of the interaction between HL and Cu^{2+} was also probed in buffered pH by the continuous variation method (Job's plot). The molar ratios between HL and Cu^{2+} in a MeOH/H_2O (1:1, v/v; HEPES, 20 mM; pH = 7.00) medium were varied with the combined

DOI: 10.1021/acsomega.8b01483
ACS Omega 2018, 3, 10471−10480

molarity fixed at 50 μM (Figure S9). The intersect between the two fitted linear sections was determined at a molar fraction of 0.50, confirming the 1:1 stoichiometry of HL interaction with Cu^{2+} observed above and also in agreement with the results from the ESI-HRMS (Figure S10) and Cu^{2+} titration experiments (see below).

In order to determine the sensitivity of HL toward Cu^{2+} a metal titration experiment was conducted in buffered pH, in which 5 μL additions of $CuCl_2$ in aqueous solution were added to a cuvette with 20 μM of HL dissolved in a MeOH/H_2O (1:1, v/v; HEPES, 20 mM; pH = 7.00) mixture (Figure 4). Upon the addition of Cu^{2+} up to 20 μM, a directly proportionate increase in the band at 408 nm was observed. An isosbestic point was observed at 346 nm, occurring between the peak maximum for HL (~320 nm) and that for the complex (408 nm), indicating a formation via a single equilibrium step. Furthermore, after 20 μM had been added, no further spectrophotometric change was observed, indicating saturation of HL with 1 equiv of Cu^{2+}. This is in good agreement with the 1:1 stoichiometry found above. A linear relationship was observed on plotting the ratio between the complex peak maximum and the isosbestic point (408 nm/346 nm) absorptions versus the effective Cu^{2+} concentration, indicating that this spectrophotometric change is ratiometric and thus can be used to estimate the concentration of Cu^{2+} independently of the HL concentration. The limit of detection (LoD) and limit of quantification (LoQ) were calculated from this ratiometric change of 408/346 nm, yielding outstanding values of 3.7 nM and 12.4 nM respectively. To the best of our knowledge, HL proves to be one of the most sensitive UV−vis-based chemosensors for Cu^{2+} detection and is comparable to some of the highest sensitivity fluorescence-based sensors so far reported (Table 1).

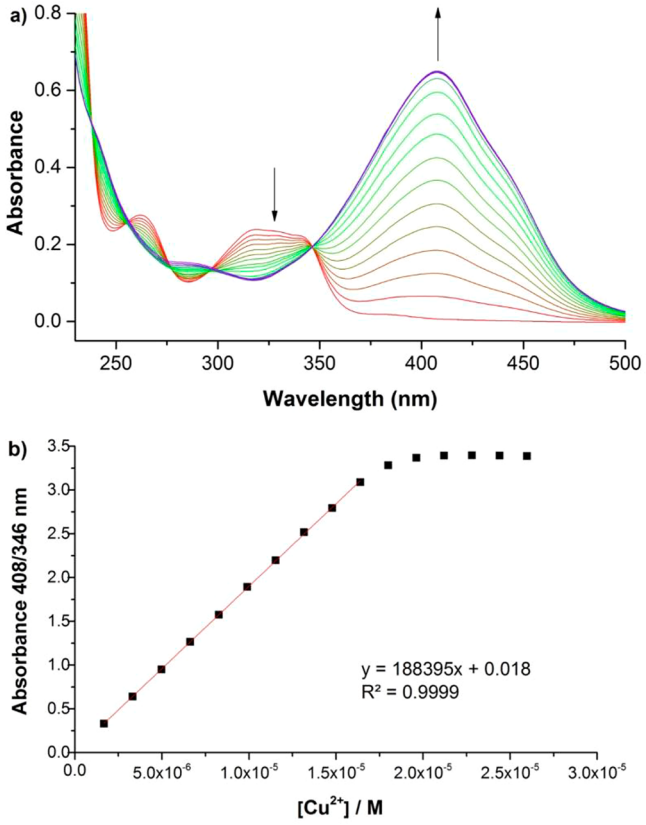

Figure 4. (a) Absorption spectral change of HL (20 μM) upon titration with $CuCl_2$ in a MeOH/H_2O (1:1, v/v; HEPES, 20 mM; pH = 7.00) mixture. The peak associated with formation of the complex is at λ_{max} = 408 nm. (b) The linear plot used for LoD and LoQ calculations was obtained by plotting the absorbance ratio of the complex band over the isosbestic peak.

To assess the naked-eye Cu^{2+} detection ability of HL, we added increasing aliquots of Cu^{2+} to 20 μM samples of HL prepared in a MeOH/H_2O (1:1, v/v; HEPES, 20 mM; pH = 7.00) mixture and found that the presence of Cu^{2+} becomes visually detectable at as low as 1.5 μM and is clearly evident from 2.5 μM (Figure 5).

Cu^{2+} Detection Selectivity and Reversibility. The selectivity of HL for Cu^{2+} was also probed in the presence of competing cations; UV−vis experiments were conducted in which Cu^{2+} complexation was investigated in solutions containing an excess of a competing metal ion. This was carried out in a MeOH/H_2O (1:1, v/v; HEPES, 20 mM; pH = 7.00) medium, where HL was present at 20 μM, Cu^{2+} at 1 equiv (20 μM), and a competing cation in a 4 equiv (80 μM) excess (see UV−vis spectra Figure S11). As shown in Figure 6a, the selectivity of HL for Cu^{2+} is unaffected by the presence of any of the competing cations employed. In each case, the solution color observed by the naked-eye is in good agreement with the UV−vis measurements, with all solutions exhibiting a yellow color associated with formation of the Cu^{2+} complex (Figure 6b).

Reversibility studies employing ethylenediaminetetraacetic acid disodium salt (H_2Na_2EDTA) were undertaken in order to probe the robustness of HL with respect to its repetitive binding to Cu^{2+}. As with previous experiments, HL was prepared as a 20 μM solution in a MeOH/H_2O (1:1, v/v; HEPES, 20 mM; pH = 7.00) mixture. Initially Cu^{2+} was added at 1 equiv (20 μM), followed by 4 equiv (80 μM) of $EDTA^{4-}$. Subsequent cycles were undertaken by adding a further 80 μM of Cu^{2+} followed by 80 μM of $EDTA^{4-}$ (Figure 7). The addition of $EDTA^{4-}$ results in the disappearance of the band at 408 nm, while the further addition of an excess of Cu^{2+} results in the reformation of this band. As the absorbance peak (λ_{max} = 408 nm) was not significantly affected after several cycling events, this result indicates that HL is suitable as a reversible sensor.

Structural Study of the Cu^{2+} Complex. In order to probe the binding mode of HL to Cu^{2+}, we focused on the visible and EPR spectra of the complex. The EPR spectra of frozen complex solutions in buffered MeOH/H_2O (1:1, v/v; HEPES, 20 mM; pH = 7.00) media, in the absence and also in the presence of additional O- or N-donor atoms (respectively, DMSO or pyridine, Figure 8), all unambiguously display a single species of rhombic symmetry and a $d_{x^2-y^2}$ ground state, consistent with elongated rhombic-octahedral or distorted square-based pyramidal stereochemistry.[64] The *A* hyperfine coupling constants and *g* factors of these complex samples obtained by spectral simulation (Table 3) are indicative of either N_3O or N_2O_2 equatorial coordination donor sets as seen from the values of g_3 and A_3,[65] pointing to involvement of one O and 2 N donor atoms from HL on the equatorial positions of the complex. Additionally, the visible spectra obtained for samples under similar conditions to those used for the EPR study (Figure S12) display two distinguishable absorptions (as shoulders of the higher energy one) centered at the 610−620 and 730−750 nm regions, a feature that has been assigned to Cu^{2+} complexes of square pyramidal geometry featuring strong axial bonding interaction.[66,67] Thus, we propose that these spectroscopic results are in accord with HL forming a distorted square pyramidal complex in solution by coordination of Cu^{2+} to the phenoxyl O and both

DOI: 10.1021/acsomega.8b01483
ACS Omega 2018, 3, 10471−10480

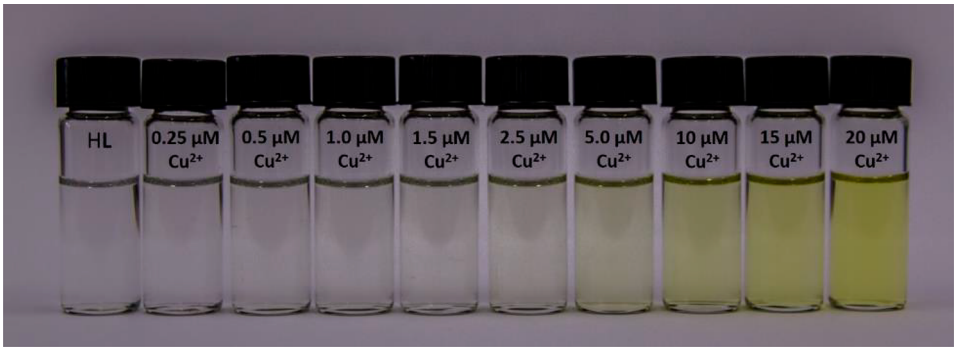

Figure 5. Detection of Cu^{2+} by the naked eye at 20 μM of HL in MeOH/H_2O (1:1, v/v; HEPES, 20 mM; pH = 7.00) with increasing concentrations of $CuCl_2$.

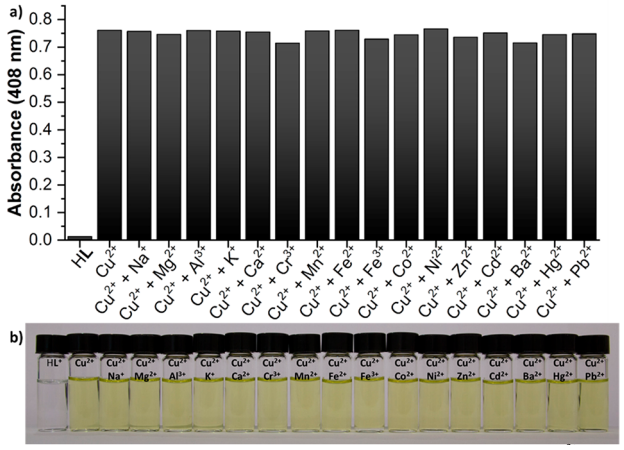

Figure 6. (a) Competing ion study with HL (20 μM) and 1 equiv (20 μM) of Cu^{2+} in the presence of 4 equiv (80 μM) of other metal ions in a MeOH/H_2O (1:1, v/v; HEPES, 20 mM; pH = 7.00) medium at λ_{max} = 408 nm. (b) Competing ion solutions as visible to the naked-eye; the detection of Cu^{2+} by the observed color change to yellow remains unaffected by other metal ions.

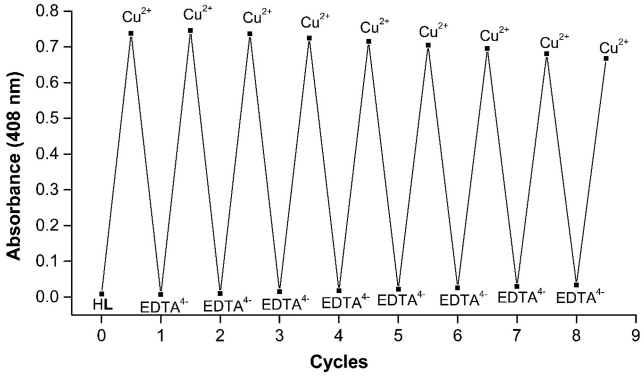

Figure 7. Reversibility of the response of HL (20 μM) in a MeOH/H_2O (1:1, v/v; HEPES, 20 mM; pH = 7.00) mixture at λ_{max} = 408 nm after cycling with additions of Cu^{2+} (20 μM initially, 80 μM thereafter) and $EDTA^{4-}$ (80 μM).

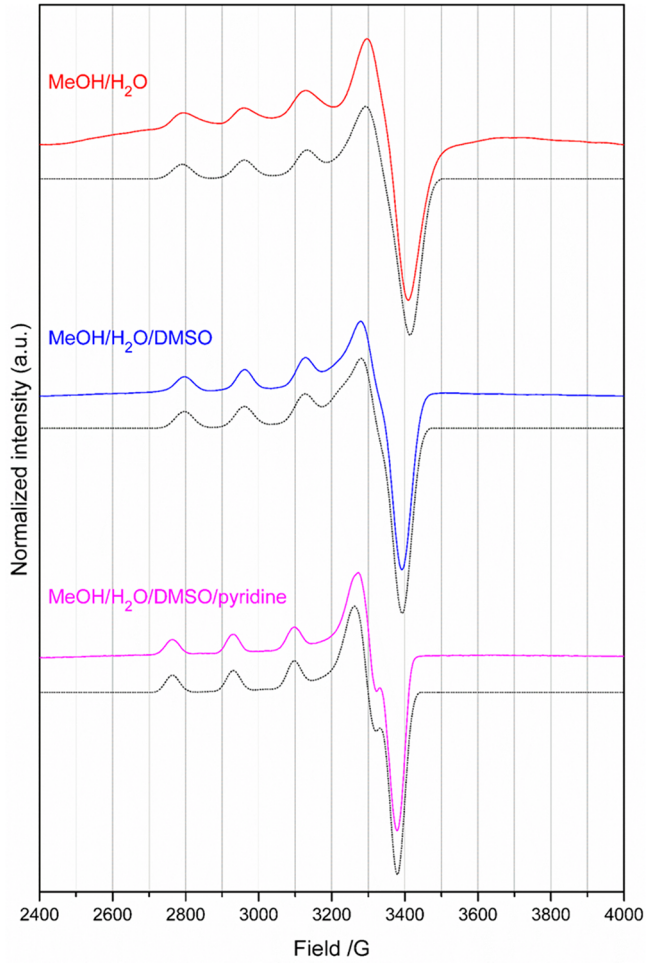

Figure 8. EPR spectra of the complex of HL with Cu^{2+} in different buffered media (HEPES, 20 mM; pH = 7.00); dotted lines are the corresponding simulated spectra.

secondary amine N atoms to define an approximate equatorial coordination plane, with additional donors from the media completing the coordination sphere at the remaining equatorial and axial positions of the metal center.

Detection of Cu^{2+} in Tap Water. To evaluate the sensing potential of HL in real world samples, two tap waters suitable for human consumption were taken from the Sydney area in New South Wales, Australia. A third sample of known concentration (5 μM of $CuCl_2$) was prepared using Milli-Q water and a standardized Cu^{2+} solution. These samples were prepared in a MeOH/H_2O (1:1, v/v; HEPES, 20 mM; pH = 7.00) buffered media with HL at 20 μM. The samples were analyzed using UV−vis, and the ratio of their absorbance at 408/346 nm plotted against a linear calibration plot (Figures S13 and S14). As shown in Table 4, the measured 5 μM spike of each tap water, and the 5 μM laboratory prepared water sample are in good agreement with the expected values. Thus, HL is suitable for the quantitative detection of Cu^{2+} far below the WHO guidelines of 2 mg/L (31.5 μM).

DOI: 10.1021/acsomega.8b01483
ACS Omega 2018, 3, 10471−10480

Table 3. Spectroscopic Data for the Cu^{2+} Complex of HL Prepared in Different (pH = 7 Buffered) Aqueous Media

medium	visible absorption,[a] λ_{max} (ε)	EPR parameters[b]					
		g_1	g_2	g_3	A_1	A_2	A_3
MeOH/H_2O 1:1	615 sh (712), 745 sh (527)	2.020	2.048	2.230	<5	24.4	176.8
MeOH/H_2O/DMSO 2:2:1	612 sh (724), 750 sh (530)	2.042	2.068	2.253	10.0	20.2	175.2
MeOH/H_2O/DMSO/pyridine 50:50:25:1	614 sh (999), 735 sh (779)	2.035	2.061	2.232	<5	29.8	170.9

[a]At 25 °C, λ_{max} in nm and ε in M^{-1} cm^{-1}. [b]In frozen solutions at 130 K, A_i is given in 10^{-4} cm^{-1}.

Table 4. Determination of Cu^{2+} in Water Samples (n = 5)

sample	Cu^{2+} added (μM)	Cu^{2+} found (μM)	recovery (%)	RSD (%)
tap 1	0.00	8.57		0.85
	5.00	13.62	100.34	0.82
tap 2	0.00	4.19		0.26
	5.00	9.13	99.38	1.14
laboratory prepared water	5.00	4.95	99.07	1.14

CONCLUSIONS

In summary, we report an efficient colorimetric Cu^{2+} chemosensor for use in aqueous methanol media. The sensor HL exhibits an excellent ratiometric response, also visible by the naked-eye, corresponding to a clear color change from colorless to yellow. In addition, Cu^{2+} sensing is selective, being unaffected by the presence of the wide range of other metal cations tested. In buffered medium at pH = 7, an outstanding 3.7 nM limit of detection for Cu^{2+} was obtained in the low nanomolar range, one of the most sensitive reported in aqueous media. Furthermore, the reaction stoichiometry between HL and Cu^{2+} was unambiguously established as 1:1, and the complexation is reversible employing $EDTA^{4-}/Cu^{2+}$ cycling. The coordination geometry of the formed complex was also tentatively assigned as square pyramidal. The complexation constants determined from the pH titrations point to the formation of a thermodynamically stable complex that exists almost exclusively as [CuL(OH)] in the range of pH = 5−8. According to the preliminary results, the simplicity and effectiveness of this sensor show great potential for real word applications in Cu^{2+} detection via qualitative (visible color change) and quantitative (spectrophotometric) methods.

MATERIALS AND METHODS

Chemicals and Reagents. All chemicals and solvents were of commercial grade and used without further purification. All aqueous solutions were prepared with type I water from a Milli-Q water purification system. Metal standards were prepared from chloride (Na^+, Mg^{2+}, Al^{3+}, K^+, Ca^{2+}, Cr^{3+}, Mn^{2+}, Fe^{2+}, Fe^{3+}, Co^{2+}, Ni^{2+}, Cu^{2+}, Zn^{2+}, Cd^{2+}, Ba^{2+} and Hg^{2+}) or nitrate salts (Pb^{2+}) of analytical grade, then standardized using literature complexometric titration methods with H_2Na_2EDTA.[68]

Synthesis of HL. The preparation of HL was optimized from a literature procedure (Scheme 1).[69] In a 50 mL round-bottom flask, 4-(diethylamino)salicylaldehyde (1000 mg, 5.2 mmol), 1,8-diaminonaphthalene (825 mg, 5.2 mmol), and a catalytic amount of *p*-toluenesulfonic acid (PTSA) were combined and dissolved in isopropanol (30 mL). This mixture was heated at 65 °C for 24 h, and the resulting precipitate was filtered and washed with 50% isopropanol (H_2O/isopropanol, v/v). The product was then dried under vacuum at 40 °C, yielding 1.4 g (82%) of HL as a white crystalline powder. Crystals suitable for SC-XRD were grown by slow evaporation of HL in an ethanol/acetone mixture (1:4 v/v). ^1H NMR (DMSO-d_6 with TMS, 300 MHz) δ (ppm) 9.16 (s. 1H), 7.22 (d. 1H), 7.13 (t. 2H), 6.98 (d. 2H), 6.51 (d. 2H), 6.43 (s. 2H), 6.20 (s. 1H), 6.18 (s. 1H), 5.50 (s. 1H), 3.29 (q. 4H), 1.07 (t. 6H). ^{13}C NMR (DMSO-d_6 with TMS, 75.5 MHz) δ (ppm) 156.36, 148.37, 143.71, 134.34, 129.24, 126.63, 115.07,113.57, 112.50, 104.36, 102.99, 98.31, 61.22, 43.76, 12.39. ESI-HRMS (positive-ion detection, MeOH, m/z): calculated for $[HL + H]^+$, 334.1919; found, 334.1884. FT-IR (ATR ν_{max}/cm^{-1}): 3333, 2966, 1596, 1562, 1411, 1216, 1118, 818, 761. Melting point: 156.7 °C. UV−vis (1 cm optical path length, MeOH−H_2O, 1/1, v/v, HEPES 20 mM, pH = 7.00): 20 μM HL, λ_{max} = 320 nm (abs = 0.277, ε = 13 850), 262 nm (abs = 0.324, ε = 16 200).

General Methods. Characterization of HL was carried out using a range of techniques. ^1H and ^{13}C NMR spectra were measured on a Bruker DRX-300 NMR spectrometer. FT-IR measurements were conducted on a Bruker Vertex 70 spectrometer. High resolution electrospray ionization mass spectra (ESI-HRMS) were collected using a Waters Xevo QToF quadrupole mass spectrometer with samples dissolved in methanol. Simultaneous thermal analysis (STA) was undertaken on a Netzsch STA449 C Jupiter thermo-microbalance. A PerkinElmer Lambda 45 UV−vis spectrophotometer was used to conduct the Job's plot and titration experiments, while all other UV−vis works were performed using a Varian Cary 100 spectrophotometer. Quartz cuvettes with a 1 cm optical path length were used for all UV−vis measurements. Single crystal X-ray diffraction (SC-XRD) was undertaken at the Australian Synchrotron on the MX1 beamline at 100(2) K with silicon double crystal monochromated radiation.[70] Data collection was through Blu-Ice[71] software, with data integration and reduction undertaken using XDS;[72] following this, an empirical absorption correction was applied using SADABS software.[73] The crystal structure was solved by direct methods, and the full-matrix least-squares refinements were conducted using the SHELX[74,75] suite of programs via Olex2 interface.[76]

UV−Vis Spectroscopy. A 2.00 mM stock solution of HL was prepared in MeOH; this solution was used for all spectroscopic experiments. Metal interaction studies were conducted using 20 μM HL in a MeOH/H_2O (1:1, v/v, HEPES 20 mM, pH = 7.00) buffered mixture with 2 equiv (40 μM) of various chloride and nitrate salts. Competing ion studies were prepared with a similar mixture, 20 μM HL in a MeOH/H_2O (1:1, v/v, HEPES 20 mM, pH = 7.00) mixture. $CuCl_2$ was added as 1 equiv (20 μM), with competing metal ions added in a higher excess (80 μM). Job's plot measurements were undertaken using literature protocols,[77,78] where HL and Cu^{2+} were prepared in various molar ratios, with the combined concentration of both at 50 μM in all analytical solutions. These molar ratio mixtures were prepared in a MeOH/H_2O (1:1, v/v, HEPES 20 mM, pH = 7.00) buffered mixture.

The complex formed by HL and Cu^{2+} was studied in more detail in the visible range using higher concentration samples in both the absence and the presence of additional coordinating compounds, namely, DMSO as a good O-donor and pyridine as a good N-donor. These were prepared in buffered aqueous

DOI: 10.1021/acsomega.8b01483
ACS Omega 2018, 3, 10471−10480

medium (HEPES 20 mM, pH = 7.00) containing both HL and Cu^{2+} at a 1:1 concentration ratio in the 0.78−1.0 mM range in the following solvent mixtures (v/v): (a) MeOH/H_2O 1:1, (b) MeOH/H_2O/DMSO 2:2:1, and (c) MeOH/H_2O/DMSO/pyridine 50:50:25:1. In these spectra, the relevant bands (600−800 nm) appear as shoulders on the more energetic band at ∼410 nm, so the maxima of these absorptions were determined employing the second-derivative method.

EPR Spectroscopy Studies. The electron paramagnetic resonance spectra were measured on a Bruker EMX 300 spectrometer operating at the X-band and equipped with a continuous-flow cryostat for liquid nitrogen. Here, the complex formed by HL with Cu^{2+} was also studied in the absence and in the presence of additional coordinating compounds, similar to the procedure used for visible absorption studies. The samples were prepared in buffered aqueous mixtures (HEPES 20 mM, pH = 7.00) containing both HL and Cu^{2+} at a 1:1 concentration ratio in the 0.20−0.48 mM range in the following solvent mixtures (v/v): (a) MeOH/H_2O 1:1, (b) MeOH/H_2O/DMSO 2:2:1, and (c) MeOH/H_2O/DMSO/pyridine 50:50:25:1. The EPR spectra of the frozen sample solutions were acquired at 130 K at a microwave power of 2.0 mW and a frequency of 9.5 GHz. The experimental spectra were then simulated using the SpinCount software[79] in order to obtain the corresponding *g* factors and *A* hyperfine coupling constants. All spectra were successfully simulated considering the presence of a single paramagnetic complex species.

Equilibrium Studies. The equilibrium constants for the protonation of HL and the formation of its Cu^{2+} complexes were determined by UV−vis pH titrations in the range of pH = 3−11. The experimental setup used in these titrations consisted of a closed titration vessel of 5−70 mL volume with thermostat jacket set on top of a 801 magnetic stirrer and connected to a Dosimat Plus 865 buret, all from Metrohm, as well as being coupled to a Haake F3 thermostatic water circulator for temperature control. All experiments were performed at 25 ± 0.1 °C in MeOH/H_2O (1:1, v/v) medium at 0.10 ± 0.01 M in KCl, using standardized KOH solutions in MeOH/H_2O (1:1, v/v) as titrant (at ca. 0.10 M for protonation and 0.02 M for complexation); a nitrogen atmosphere was maintained in the titration vessel. The KOH titrant solutions were prepared from dilution of a commercial ampule and standardized using Gran's method.[80] The starting solutions for titrations contained KCl at 0.10 M, HCl at 1.0×10^{-3} M (for pH ≈ 3.0), HL at 2.5×10^{-5} M (and $CuCl_2$ in equimolar amount in the case of complexation), all in a starting volume of 20 mL. After each titrant addition, a sample of ca. 1 mL was taken from the titration solution, placed in a 1 cm Hellma 114-QS cuvette and measured on a PerkinElmer lambda 45 UV−vis spectrometer, after which the sample was returned to the titration solution. The pH was not measured experimentally; instead the proton concentration was calculated from the addition volumes and concentrations of the titrant solutions. The titration data were fitted using the HypSpec software,[81] in the range of 240−370 nm in the absence of Cu^{2+} or of 370−500 nm in the presence of Cu^{2+}. Species distribution diagrams were plotted with the HySS software at 25 μM of HL.[82]

Sensitivity Studies of HL with Cu^{2+}. To determine the sensitivity of HL to Cu^{2+}, a metal titration approach was used in buffered pH, where 5 μL additions of $CuCl_2$ aqueous solution were added to a cuvette with 20 μM of HL dissolved in a MeOH/H_2O (1:1, v/v; HEPES, 20 mM; pH = 7.00) mixture, until no further spectral shift was observed. The limit of detection (LoD) and limit of quantification (LoQ) were calculated using $3\sigma/m$ and $10\sigma/m$, respectively,[83] where σ is the standard deviation of a blank solution and *m* is the slope of the linear plot obtained. For the standard deviation (σ) determination, we took 10 repeated spectra measurements of a blank solution (HL solution in the same conditions used for measurements but without any addition of Cu^{2+}) and calculated the standard deviation for the absorbance values at 408 nm, obtaining a value of $\sigma = 2.34 \times 10^{-4}$.

Detection of Cu^{2+} in Tap Water. Tap water samples were taken from residential drinking taps in southeast (tap 1) and northwest (tap 2) Sydney, New South Wales, Australia. An additional sample of a known Cu^{2+} concentration (5 μM) was prepared in Milli-Q water. To probe the accuracy and precision of HL, tap water solutions were also spiked with 5 μM of Cu^{2+}, and all samples were measured with 5 replicates.

Quantitative detection of Cu^{2+} in these samples was carried out by UV−vis spectroscopy with HL (20 μM) in a MeOH/H_2O (1:1, v/v; HEPES, 20 mM; pH = 7.00) buffered media. The ratiometric response taken from 408/346 nm was plotted against a calibration curve in the same media. As the water sample was 40% of the total in cuvette volume, a correction for sample dilution was applied.

■ ASSOCIATED CONTENT

Supporting Information

The Supporting Information is available free of charge on the ACS Publications website at DOI: 10.1021/acsomega.8b01483.

Crystallographic structure of HL (CIF)

Additional characterization details of HL and binding studies including ^1H and ^{13}C NMR, ESI-HRMS, STA, FT-IR, various UV−vis experiments, and crystallographic data (PDF)

■ AUTHOR INFORMATION

Corresponding Authors

*E-mail: feng.li@westernsydney.edu.au (F.L.).

*E-mai: j.reynolds@westernsydney.edu.au (J.K.R.).

ORCID

Luís M. P. Lima: 0000-0002-9729-330X

Feng Li: 0000-0001-8465-9678

Notes

The authors declare no competing financial interest.

CCDC-1820800 contains details of the crystallographic data for this article; these data can be obtained free of charge from the Cambridge Crystallographic Data Centre via www.ccdc.cam.ac.uk/data_request/cif.

■ ACKNOWLEDGMENTS

The authors thank the Western Sydney University (WSU) Advance Material Characterisation Facility and the WSU Mass Spectrometry Facility for instrumental access. D.J.F. thanks WSU for a Postgraduate Research Award and CSIRO for a Ph.D. top-up award. L.M.P.L. is grateful for financial support from project LISBOA-01-0145-FEDER-007660 (Microbiologia Molecular, Estrutural e Celular) funded by FEDER funds through COMPETE2020-Programa Operacional Competitividade e Internacionalização (POCI) and by national funds through Fundação para a Ciência e a Tecnologia (FCT) and also for a postdoctoral fellowship (SFRH/BPD/73361/2010) from FCT. The crystallographic data acquisition was undertaken on the MX1 beamline at the Australian Synchrotron, Clayton, Victoria,

DOI: 10.1021/acsomega.8b01483
ACS Omega 2018, 3, 10471−10480

Australia. We also thank the Australian Synchrotron for travel funding and their beamline scientists for beamline assistance.

REFERENCES

(1) Steed, J. W.; Atwood, J. L.; Gale, P. A. Definition and Emergence of Supramolecular Chemistry. In *Supramolecular Chemistry: From Molecules to Nanomaterials*; Gale, P. A., Steed, J. W., Eds.; Wiley: Chichester, U.K., 2012; pp 3−9.

(2) Gloe, K.; Gloe, K.; Wenzel, M.; Lindoy, L. F.; Li, F. Supramolecular Chemistry in Solvent Extraction: Toward Highly Selective Extractants and a Better Understanding of Phase-Transfer Phenomena. In *Ion Exchange and Solvent Extraction*; Moyer, B. A., Ed.; CRC Press: Boca Raton, FL, 2013; Vol. *21*, pp 1−48.

(3) Gale, P. A.; Caltagirone, C. Fluorescent and Colorimetric Sensors for Anionic Species. *Coord. Chem. Rev.* **2018**, *354*, 2−27.

(4) Kaur, B.; Kaur, N.; Kumar, S. Colorimetric Metal Ion Sensors − A Comprehensive Review of the Years 2011−2016. *Coord. Chem. Rev.* **2018**, *358*, 13−69.

(5) Aulsebrook, M. L.; Graham, B.; Grace, M. R.; Tuck, K. L. Lanthanide Complexes for Luminescence-Based Sensing of Low Molecular Weight Analytes. *Coord. Chem. Rev.* **2017**, DOI: 10.1016/j.ccr.2017.11.018.

(6) Wu, D.; Sedgwick, A. C.; Gunnlaugsson, T.; Akkaya, E. U.; Yoon, J.; James, T. D. Fluorescent Chemosensors: The Past, Present and Future. *Chem. Soc. Rev.* **2017**, *46* (23), 7105−7123.

(7) Sakai, R.; Satoh, T.; Kakuchi, T. Polyacetylenes as Colorimetric and Fluorescent Chemosensor for Anions. *Polym. Rev.* **2017**, *57* (1), 159−174.

(8) Pan, J.; Tang, F.; Ding, A.; Kong, L.; Yang, L.; Tao, X.; Tian, Y.; Yang, J. A Small-Molecule Chemosensor for the Selective Detection of 2,4,6-Trinitrophenol (TNP). *RSC Adv.* **2015**, *5* (1), 191−195.

(9) Shanmugaraju, S.; Mukherjee, P. S. *π*-Electron Rich Small Molecule Sensors for the Recognition of Nitroaromatics. *Chem. Commun.* **2015**, *51* (89), 16014−16032.

(10) Lin, V. S.; Chen, W.; Xian, M.; Chang, C. J. Chemical Probes for Molecular Imaging and Detection of Hydrogen Sulfide and Reactive Sulfur Species in Biological Systems. *Chem. Soc. Rev.* **2015**, *44* (14), 4596−4618.

(11) Butler, S. J.; Parker, D. Anion Binding in Water at Lanthanide Centres: From Structure and Selectivity to Signalling and Sensing. *Chem. Soc. Rev.* **2013**, *42* (4), 1652−1666.

(12) Esipenko, N. A.; Koutnik, P.; Minami, T.; Mosca, L.; Lynch, V. M.; Zyryanov, G. V.; Anzenbacher, P. First Supramolecular Sensors for Phosphonate Anions. *Chem. Sci.* **2013**, *4* (9), 3617−3623.

(13) Bernier, N.; Carvalho, S.; Li, F.; Delgado, R.; Félix, V. Anion Recognition by a Macrobicycle Based on a Tetraoxadiaza Macrocycle and an Isophthalamide Head Unit. *J. Org. Chem.* **2009**, *74* (13), 4819−4827.

(14) Li, F.; Delgado, R.; Drew, M. G. B.; Felix, V. Dioxadiaza- and Trioxadiaza-Macrocycles Containing One Dibenzofuran Unit Selective for Cadmium. *Dalton Trans.* **2006**, No. 45, 5396−5403.

(15) Vázquez, M.; Fabbrizzi, L.; Taglietti, A.; Pedrido, R. M.; González-Noya, A. M.; Bermejo, M. R. A Colorimetric Approach to Anion Sensing: A Selective Chemosensor of Fluoride Ions, in Which Color Is Generated by Anion-Enhanced *π* Delocalization. *Angew. Chem.* **2004**, *116* (15), 1996−1999.

(16) Wallace, K. J.; Belcher, W. J.; Turner, D. R.; Syed, K. F.; Steed, J. W. Slow Anion Exchange, Conformational Equilibria, and Fluorescent Sensing in Venus Flytrap Aminopyridinium-Based Anion Hosts. *J. Am. Chem. Soc.* **2003**, *125* (32), 9699−9715.

(17) Xuan, W.; Pan, R.; Wei, Y.; Cao, Y.; Li, H.; Liang, F.-S.; Liu, K.-J.; Wang, W. Reaction-Based "Off−On" Fluorescent Probe Enabling Detection of Endogenous Labile Fe^{2+} and Imaging of Zn^{2+}-Induced Fe^{2+} Flux in Living Cells and Elevated Fe^{2+} in Ischemic Stroke. *Bioconjugate Chem.* **2016**, *27* (2), 302−308.

(18) Wang, C.; Liu, Y.; Cheng, J.; Song, J.; Zhao, Y.; Ye, Y. Efficient FRET-Based Fuorescent Ratiometric Chemosensors for Fe^{3+} and Its Application in Living Cells. *J. Lumin.* **2015**, *157*, 143−148.

(19) Maniyazagan, M.; Mariadasse, R.; Jeyakanthan, J.; Lokanath, N. K.; Naveen, S.; Premkumar, K.; Muthuraja, P.; Manisankar, P.; Stalin, T. Rhodamine Based "Turn−on" Molecular Switch FRET−Sensor for Cadmium and Sulfide Ions and Live Cell Imaging Study. *Sens. Actuators, B* **2017**, *238*, 565−577.

(20) Aich, K.; Goswami, S.; Das, S.; Mukhopadhyay, C. D.; Quah, C. K.; Fun, H.-K. Cd^{2+} Triggered the FRET "ON": A New Molecular Switch for the Ratiometric Detection of Cd^{2+} with Live-Cell Imaging and Bound X-Ray Structure. *Inorg. Chem.* **2015**, *54* (15), 7309−7315.

(21) Vengaian, K. M.; Britto, C. D.; Sekar, K.; Sivaraman, G.; Singaravadivel, S. Fluorescence "on−off−on" Chemosensor for Selective Detection of Hg^{2+} and S^{2-}: Application to Bioimaging in Living Cells. *RSC Adv.* **2016**, *6* (9), 7668−7673.

(22) Song, J.; Huai, M.; Wang, C.; Xu, Z.; Zhao, Y.; Ye, Y. A New FRET Ratiometric Fluorescent Chemosensor for Hg^{2+} and Its Application in Living EC 109 Cells. *Spectrochim. Acta, Part A* **2015**, *139*, 549−554.

(23) Li, D.; Sun, X.; Huang, J.; Wang, Q.; Feng, Y.; Chen, M.; Meng, X.; Zhu, M.; Wang, X. A Carbazole-Based "Turn-on" Two-Photon Fluorescent Probe for Biological Cu^{2+} Detection Vis Cu^{2+}-Promoted Hydrolysis. *Dyes Pigm.* **2016**, *125*, 185−191.

(24) Li, M.; Sun, Y.; Dong, L.; Feng, Q.-C.; Xu, H.; Zang, S.-Q.; Mak, T. C. Colorimetric Recognition of Cu^{2+} and Fluorescent Detection of Hg^{2+} in Aqueous Media by a Dual Chemosensor Derived from Rhodamine B Dye with a NS 2 Receptor. *Sens. Actuators, B* **2016**, *226*, 332−341.

(25) Yin, S.; Leen, V.; Van Snick, S.; Boens, N.; Dehaen, W. A Highly Sensitive, Selective, Colorimetric and near-Infrared Fluorescent Turn-on Chemosensor for Cu^{2+} Based on BODIPY. *Chem. Commun.* **2010**, *46* (34), 6329−6331.

(26) He, X.; Zhang, J.; Liu, X.; Dong, L.; Li, D.; Qiu, H.; Yin, S. A Novel BODIPY-Based Colorimetric and Fluorometric Dual-Mode Chemosensor for Hg^{2+} and Cu^{2+}. *Sens. Actuators, B* **2014**, *192*, 29−35.

(27) *Trace Elements in Human Health and Disease*; Prasad, A. S., Oberleas, D., Eds.; Academic Press: New York, 1976.

(28) Uauy, R.; Olivares, M.; Gonzalez, M. Essentiality of Copper in Humans. *Am. J. Clin. Nutr.* **1998**, *67* (5), 952S−959S.

(29) Aust, S. D.; Morehouse, L. A.; Thomas, C. E. Role of Metals in Oxygen Radical Reactions. *J. Free Radicals Biol. Med.* **1985**, *1* (1), 3−25.

(30) Gaggelli, E.; Kozlowski, H.; Valensin, D.; Valensin, G. Copper Homeostasis and Neurodegenerative Disorders (Alzheimer's, Prion, and Parkinson's Diseases and Amyotrophic Lateral Sclerosis). *Chem. Rev.* **2006**, *106* (6), 1995−2044.

(31) Bull, P. C.; Thomas, G. R.; Rommens, J. M.; Forbes, J. R.; Cox, D. W. The Wilson Disease Gene Is a Putative Copper Transporting P−Type ATPase Similar to the Menkes Gene. *Nat. Genet.* **1993**, *5* (4), 327−337.

(32) de Bie, P.; Muller, P.; Wijmenga, C.; Klomp, L. W. J. Molecular Pathogenesis of Wilson and Menkes Disease: Correlation of Mutations with Molecular Defects and Disease Phenotypes. *J. Med. Genet.* **2007**, *44* (11), 673−688.

(33) World Health Organization. *Guidelines for Drinking-Water Quality*, 4th ed.; World Health Organization: Geneva, 2011.

(34) You, G. R.; Jang, H. J.; Jo, T. G.; Kim, C. A Novel Displacement-Type Colorimetric Chemosensor for the Detection of Cu $^{2+}$ and GSH in Aqueous Solution. *RSC Adv.* **2016**, *6* (78), 74400−74408.

(35) Noh, J. Y.; Park, G. J.; Na, Y. J.; Jo, H. Y.; Lee, S. A.; Kim, C. A Colorimetric "Naked-Eye" Cu(II) Chemosensor and pH Indicator in 100% Aqueous Solution. *Dalton Trans.* **2014**, *43* (15), 5652−5656.

(36) Kang, J. H.; Lee, S. Y.; Ahn, H. M.; Kim, C. Sequential Detection of Copper(II) and Cyanide by a Simple Colorimetric Chemosensor. *Inorg. Chem. Commun.* **2016**, *74*, 62−65.

(37) Elmorsi, T. M.; Aysha, T. S.; Machalický, O.; Mohamed, M. B. I.; Bedair, A. H. A Dual Functional Colorimetric and Fluorescence Chemosensor Based on Benzo[f]Fluorescein Dye Derivatives for Copper Ions and PH; Kinetics and Thermodynamic Study. *Sens. Actuators, B* **2017**, *253*, 437−450.

(38) Lee, S. Y.; Bok, K. H.; Kim, J. A.; Kim, S. Y.; Kim, C. Simultaneous Detection of Cu^{2+} and Cr^{3+} by a Simple Schiff-Base Colorimetric

DOI: 10.1021/acsomega.8b01483
ACS Omega 2018, 3, 10471−10480

Chemosensor Bearing NBD (7-Nitrobenzo-2-Oxa-1, 3-Diazolyl) and Julolidine Moieties. *Tetrahedron* **2016**, *72* (35), 5563−5570.
(39) Kim, M. S.; Jo, T. G.; Ahn, H. M.; Kim, C. A Colorimetric and Fluorescent Chemosensor for the Selective Detection of Cu^{2+} and Zn^{2+} Ions. *J. Fluoresc.* **2017**, *27* (1), 357−367.
(40) Kumawat, L. K.; Kumar, M.; Bhatt, P.; Sharma, A.; Asif, M.; Gupta, V. K. An Easily Accessible Optical Chemosensor for Cu^{2+} Based on Novel Imidazoazine Framework, Its Performance Characteristics and Potential Applications. *Sens. Actuators, B* **2017**, *240*, 365−375.
(41) Qu, L.; Yin, C.; Huo, F.; Chao, J.; Zhang, Y.; Cheng, F. A Pyridoxal-Based Dual Chemosensor for Visual Detection of Copper Ion and Ratiometric Fluorescent Detection of Zinc Ion. *Sens. Actuators, B* **2014**, *191*, 158−164.
(42) Zhang, B.; Diao, Q.; Ma, P.; Liu, X.; Song, D.; Wang, X. A Sensitive Fluorescent Probe for Cu^{2+} Based on Rhodamine B Derivatives and Its Application to Drinking Water Examination and Living Cells Imaging. *Sens. Actuators, B* **2016**, *225*, 579−585.
(43) Lin, Q.; Chen, P.; Liu, J.; Fu, Y.-P.; Zhang, Y.-M.; Wei, T.-B. Colorimetric Chemosensor and Test Kit for Detection Copper (II) Cations in Aqueous Solution with Specific Selectivity and High Sensitivity. *Dyes Pigm.* **2013**, *98* (1), 100−105.
(44) Roy, D.; Chakraborty, A.; Ghosh, R. Perimidine Based Selective Colorimetric and Fluorescent Turn-off Chemosensor of Aqueous Cu^{2+}: Studies on Its Antioxidant Property along with Its Interaction with Calf Thymus-DNA. *RSC Adv.* **2017**, *7* (64), 40563−40570.
(45) Wang, Z.; Yang, J.; Yang, Y.; Fang, H.; Xu, X.; Rui, J.; Su, F.; Xu, H.; Wang, S. A Novel Hexahydroquinazolin-2-Amine-Based Fluorescence Sensor for Cu^{2+} from Isolongifolanone and Its Biological Applications. *RSC Adv.* **2017**, *7* (53), 33263−33272.
(46) Sarkar, S.; Roy, S.; Sikdar, A.; Saha, R.; Panja, S. S. A Pyrene-Based Simple but Highly Selective Fluorescence Sensor for Cu^{2+} Ions via a Static Excimer Mechanism. *Analyst* **2013**, *138* (23), 7119−7126.
(47) Paul, S.; Ghosh, P.; Bhuyan, S.; Mukhopadhyay, S. K.; Banerjee, P. Nanomolar-Level Selective Dual Channel Sensing of Cu^{2+} and CN^{-} from an Aqueous Medium by an Opto-Electronic Chemoreceptor. *Dalton Trans.* **2018**, *47* (4), 1082−1091.
(48) Jia, H.; Yang, M.; Meng, Q.; He, G.; Wang, Y.; Hu, Z.; Zhang, R.; Zhang, Z. Synthesis and Application of an Aldazine-Based Fluorescence Chemosensor for the Sequential Detection of Cu^{2+} and Biological Thiols in Aqueous Solution and Living Cells. *Sensors* **2016**, *16* (1), 79.
(49) Naskar, B.; Modak, R.; Maiti, D. K.; Bauzá, A.; Frontera, A.; Maiti, P. K.; Mandal, S.; Goswami, S. A Highly Selective "ON−OFF" Probe for Colorimetric and Fluorometric Sensing of Cu^{2+} in Water. *RSC Adv.* **2017**, *7* (19), 11312−11321.
(50) Shan, Y.; Liu, Z.; Cao, D.; Liu, G.; Guan, R.; Sun, N.; Wang, C.; Wang, K. Coumarinic Chalcone Derivatives as Chemosensors for Cyanide Anions and Copper Ions. *Sens. Actuators, B* **2015**, *221*, 463−469.
(51) Wang, M.; Leung, K.-H.; Lin, S.; Chan, D. S.-H.; Kwong, D. W. J.; Leung, C.-H.; Ma, D.-L. A Colorimetric Chemosensor for Cu^{2+} Ion Detection Based on an Iridium(III) Complex. *Sci. Rep.* **2015**, *4*, 6794.
(52) Zhao, Y.-C.; Chen, C.; Chen, B.; Wang, P.-Y.; Wu, Z.-B.; Li, H.; Song, B.-A.; Yang, S. Tunable Fluorescent Probes for Selective Detection of Copper (II) and Sulphide with Completely Different Modes. *Sens. Actuators, B* **2017**, *241*, 168−173.
(53) Udhayakumari, D.; Velmathi, S. Naphthalene Thiourea Derivative Based Colorimetric and Fluorescent Dual Chemosensor for F^{-} and Cu^{2+}/Hg^{2+} Ions. *Supramol. Chem.* **2015**, *27* (7−8), 539−544.
(54) Udhayakumari, D.; Velmathi, S.; Chen, W.-C.; Wu, S.-P. A Dual-Mode Chemosensor: Highly Selective Colorimetric Fluorescent Probe for Cu^{2+} and F^{-} Ions. *Sens. Actuators, B* **2014**, *204*, 375−381.
(55) Liu, C.; Jiao, X.; He, S.; Zhao, L.; Zeng, X. A Highly Selective and Sensitive Fluorescent Probe for Cu^{2+} Based on a Novel Naphthalimide−Rhodamine Platform and Its Application in Live Cell Imaging. *Org. Biomol. Chem.* **2017**, *15* (18), 3947−3954.
(56) Zhu, D.; Ren, A.; He, X.; Luo, Y.; Duan, Z.; Yan, X.; Xiong, Y.; Zhong, X. A Novel Ratiometric Fluorescent Probe for Selective and Sensitive Detection of Cu^{2+} in Complete Aqueous Solution. *Sens. Actuators, B* **2017**, *252*, 134−141.
(57) Yuan, Y.; Sun, S.; Liu, S.; Song, X.; Peng, X. Highly Sensitive and Selective Turn-on Fluorescent Probes for Cu^{2+} Based on Rhodamine B. *J. Mater. Chem. B* **2015**, *3* (26), 5261−5265.
(58) Sokolowski, A.; Leutbecher, H.; Weyhermüller, T.; Schnepf, R.; Bothe, E.; Bill, E.; Hildebrandt, P.; Wieghardt, K. Phenoxyl-Copper(II) Complexes: Models for the Active Site of Galactose Oxidase. *JBIC, J. Biol. Inorg. Chem.* **1997**, *2* (4), 444−453.
(59) Thomas, F.; Jarjayes, O.; Duboc, C.; Philouze, C.; Saint-Aman, E.; Pierre, J.-L. Intramolecularly Hydrogen-Bonded versus copper(II) Coordinated Mono- and Bis-Phenoxyl Radicals. *Dalton Trans.* **2004**, No. 17, 2662−2669.
(60) Storr, T.; Verma, P.; Pratt, R. C.; Wasinger, E. C.; Shimazaki, Y.; Stack, T. D. P. Defining the Electronic and Geometric Structure of One-Electron Oxidized Copper−Bis-Phenoxide Complexes. *J. Am. Chem. Soc.* **2008**, *130* (46), 15448−15459.
(61) Sahoo, S. K.; Sharma, D.; Moirangthem, A.; Kuba, A.; Thomas, R.; Kumar, R.; Kuwar, A.; Choi, H.-J.; Basu, A. Pyridoxal Derived Chemosensor for Chromogenic Sensing of Cu^{2+} and Fluorogenic Sensing of Fe^{3+} in Semi-Aqueous Medium. *J. Lumin.* **2016**, *172*, 297−303.
(62) Qu, L.; Yin, C.; Huo, F.; Zhang, Y.; Li, Y. A Commercially Available Fluorescence Chemosensor for Copper Ion and Its Application in Bioimaging. *Sens. Actuators, B* **2013**, *183*, 636−640.
(63) Parween, A.; Mandal, T. K.; Guillot, R.; Naskar, S. Acid−Base Behavior, Electrochemical Properties and DFT Study of Redox Non-Innocent Phenol−Imidazole Ligands and Their Cu Complexes. *Polyhedron* **2015**, *99*, 34−46.
(64) Hathaway, B. J.; Billing, D. E. The Electronic Properties and Stereochemistry of Mono-Nuclear Complexes of the Copper(II) Ion. *Coord. Chem. Rev.* **1970**, *5* (2), 143−207.
(65) Peisach, J.; Blumberg, W. E. Structural Implications Derived from the Analysis of Electron Paramagnetic Resonance Spectra of Natural and Artificial Copper Proteins. *Arch. Biochem. Biophys.* **1974**, *165* (2), 691−708.
(66) Addison, A. W.; Rao, T. N.; Reedijk, J.; van Rijn, J.; Verschoor, G. C. Synthesis, Structure, and Spectroscopic Properties of Copper(II) Compounds Containing Nitrogen-Sulphur Donor Ligands; the Crystal and Molecular Structure of Aqua[1,7-Bis(N-Methylbenzimidazol-2[Prime or Minute]-Yl)-2,6-Dithiaheptane]Copper(II) Perchlorate. *J. Chem. Soc., Dalton Trans.* **1984**, No. 7, 1349−1356.
(67) Miyoshi, K.; Tanaka, H.; Kimura, E.; Tsuboyama, S.; Murata, S.; Shimizu, H.; Ishizu, K. Electrochemical and Spectroscopic Studies on Copper(II) Complexes of Macrocyclic Ligands as Models for Square-Pyramidal Metal Active Sites of Copper(II) Complexes of Bleomycin and Glutathione. *Inorg. Chim. Acta* **1983**, *78*, 23−30.
(68) Schwarzenbach, G.; Flaschka, H. *Complexometric Titrations*, 2nd ed.; Translated by Irving, H. M. N. H.; Methuen: London, 1969; pp 3−295.
(69) Latif, N.; Mishriky, N.; Assad, F. M.; Meguid, S. A. Reaction of Biologically Active β-Nitrostyrenes with o-Phenylenediamine: A New Route to the Synthesis of 2-Substituted Benzimidazoles. *Indian J. Chem. Sect. B Org. Chem. Med. Chem.* **1982**, *21B* (9), 872−874.
(70) Cowieson, N. P.; Aragao, D.; Clift, M.; Ericsson, D. J.; Gee, C.; Harrop, S. J.; Mudie, N.; Panjikar, S.; Price, J. R.; Riboldi-Tunnicliffe, A.; et al. MX1: A Bending-Magnet Crystallography Beamline Serving Both Chemical and Macromolecular Crystallography Communities at the Australian Synchrotron. *J. Synchrotron Radiat.* **2015**, *22* (1), 187−190.
(71) McPhillips, T. M.; McPhillips, S. E.; Chiu, H.-J.; Cohen, A. E.; Deacon, A. M.; Ellis, P. J.; Garman, E.; Gonzalez, A.; Sauter, N. K.; Phizackerley, R. P.; et al. Blu-Ice and the Distributed Control System: Software for Data Acquisition and Instrument Control at Macromolecular Crystallography Beamlines. *J. Synchrotron Radiat.* **2002**, *9* (6), 401−406.
(72) Kabsch, W. Automatic Processing of Rotation Diffraction Data from Crystals of Initially Unknown Symmetry and Cell Constants. *J. Appl. Crystallogr.* **1993**, *26* (6), 795−800.

DOI: 10.1021/acsomega.8b01483
ACS Omega 2018, 3, 10471−10480

(73) Sheldrick, G. M. *SADABS, a software for empirical absorption correction*, version 2.05; University of Göttingen: Göttingen, Germany, 2002.
(74) Sheldrick, G. M. A Short History of SHELX. *Acta Crystallogr., Sect. A: Found. Crystallogr.* **2008**, *64* (1), 112−122.
(75) Sheldrick, G. M. SHELXT − Integrated Space-Group and Crystal-Structure Determination. *Acta Crystallogr., Sect. A: Found. Adv.* **2015**, *71* (1), 3−8.
(76) Dolomanov, O. V.; Bourhis, L. J.; Gildea, R. J.; Howard, J. A. K.; Puschmann, H. OLEX2: A Complete Structure Solution, Refinement and Analysis Program. *J. Appl. Crystallogr.* **2009**, *42* (2), 339−341.
(77) Job, P. Formation and Stability of Inorganic Complexes in Solution. *Ann. Chim.* **1928**, *9*, 113−203.
(78) Renny, J. S.; Tomasevich, L. L.; Tallmadge, E. H.; Collum, D. B. Method of Continuous Variations: Applications of Job Plots to the Study of Molecular Associations in Organometallic Chemistry. *Angew. Chem., Int. Ed.* **2013**, *52* (46), 11998−12013.
(79) Petasis, D. T.; Hendrich, M. P. Quantitative Interpretation of Multifrequency Multimode EPR Spectra of Metal Containing Proteins, Enzymes, and Biomimetic Complexes. In *Methods in Enzymology*; Qin, P. Z., Warncke, K., Eds.; Academic Press, 2015; Vol. *563*, Chapter 8, pp 171−208.
(80) Rossotti, F. J. C.; Rossotti, H. Potentiometric Titrations Using Gran Plots: A Textbook Omission. *J. Chem. Educ.* **1965**, *42* (7), 375.
(81) Gans, P.; Sabatini, A.; Vacca, A. Determination of Equilibrium Constants from Spectrophometric Data Obtained from Solutions of Known PH: The Program pHab. *Ann. Chim.* **1999**, *89* (1−2), 45−49.
(82) Alderighi, L.; Gans, P.; Ienco, A.; Peters, D.; Sabatini, A.; Vacca, A. Hyperquad Simulation and Speciation (HySS): A Utility Program for the Investigation of Equilibria Involving Soluble and Partially Soluble Species. *Coord. Chem. Rev.* **1999**, *184* (1), 311−318.
(83) Magnusson, B. *The Fitness for Purpose of Analytical Methods: A Laboratory Guide to Method Validation and Related Topics*; Eurachem, 2014.

DOI: 10.1021/acsomega.8b01483
ACS Omega 2018, 3, 10471−10480